Extracellular Matrix Dysfunction in Sorsby Patient-Derived Retinal Pigment Epithelium

Abbi L. Engel[a], YeKai Wang[b,c], Thomas H. Khuu[a], Emily Worrall[a], Megan A. Manson[a], Kaitlen Knight[a], Aya Yanagida[a], Jian Hua Qi[d], Aravind Ramakrishnan[e], Richard G Weleber[f], Michael L. Klein[f], David J. Wilson[f], Bela Anand-Apte[d], James B. Hurley[a,g], Jianhai Du[b,c]*, Jennifer R. Chao[a]*

[a]Department of Ophthalmology, University of Washington, Seattle, WA 98109
[b]Department of Ophthalmology, West Virginia University, Morgantown, WV 26506
[c]Department of Biochemistry, West Virginia University, Morgantown, WV 26506
[d]Department of Ophthalmic Research, Cole Eye Institute & Lerner Research Institute, Cleveland Clinic Foundation, Cleveland, OH 44195
[e]Center for Blood Cancers and Oncology, St. David's South Austin Medical Center, Austin, TX 78704
[f]Casey Eye Institute, Oregon Health & Science University, Portland, OR 97201
[g]Department of Biochemistry, University of Washington, Seattle, WA 98195

*Corresponding authors: jrchao@uw.edu, 750 Republican Street, Box 358058, Seattle WA 98109 (206) 221-0594; or jianhai.du@wvumedicine.org, One Medical Center Dr., PO Box 9193, WVU Eye Institute, Morgantown, WV 26505; Phone: (304)-598-6903; Fax: (304)-598- 6928.

Running head: Sorsby Patient-Derived iPSC-RPE

Abbi Engel: Collection and/or assembly of data, data analysis and interpretation, manuscript writing
Yekai Wang: Collection and/or assembly of data, data analysis and interpretation
Thomas Khuu: Collection and/or assembly of data
Emily Worrall: Collection and/or assembly of data, data analysis and interpretation
Megan Manson: Collection and/or assembly of data
Kaitlen Knight: Collection and/or assembly of data, data analysis and interpretation
Aya Yanagida: Collection and/or assembly of data, data analysis and interpretation
Jian Hua Qi: Collection and/or assembly of data, data analysis and interpretation
Aravind Ramakrishnan: Provision of study material or patients
Richard Weleber: Provision of study material or patients
Michael Klein: Provision of study material or patients
David Wilson: Provision of study material or patients
Bela Anand-Apte: Data analysis and interpretation, manuscript writing, final approval of manuscript
James Hurley: Conception and design, manuscript writing, final approval of manuscript
Jianhai Du: Conception and design, provision of study material or patients, collection and/or assembly of data, data analysis and interpretation, manuscript writing, final approval of manuscript
Jennifer Chao: Conception and design, provision of study material or patients, collection and/or assembly of data, data analysis and interpretation, manuscript writing, final approval of manuscript

Key words: Retinal pigment epithelium, age-related macular degeneration, induced pluripotent stem cells, basal laminar drusen, fundus dystrophy pseudoinflammatory of Sorsby

Abstract

Sorsby Fundus Dystrophy (SFD) is a rare form of macular degeneration that is clinically similar to age-related macular degeneration (AMD). SFD results from mutations found in the tissue inhibitor of metalloproteinase 3 (*TIMP3*) gene. TIMP3 is secreted by the retinal pigmented epithelium (RPE) into the underlying Bruch's membrane (BrM), and it plays a critical role in maintaining extracellular matrix (ECM) homeostasis. A characteristic feature of post-mortem SFD globes is a thick layer of sub-RPE deposits overlying a disorganized BrM. Although likely central to the pathogenesis of SFD, no animal models have reproduced this phenotype. We generated induced pluripotent stem cell (iPSC)-derived RPE lines from SFD family members with the S204C TIMP3 mutation and observed that SFD RPE have highly dysregulated ECM and form large basal deposits by ~30 days in culture. The sub-RPE deposits are similar in ultrastructure and composition when compared to SFD family member globes. Mutant *TIMP3* correction by CRISPR-Cas9 gene editing in SFD iPSC RPE cells resulted in the reversal of sub-RPE calcium deposition. We found that SFD TIMP3 has decreased inhibition of secreted matrix metalloproteinases. ECM dysfunction substantially impacts cellular metabolism. Targeted metabolomics data showed that intracellular 4-hydroxyproline, a major breakdown product of collagen, is significantly elevated in SFD RPE. Further, SFD RPE also has decreased intracellular reduced glutathione and is more vulnerable to oxidative stress. These findings suggest that key elements of SFD pathology can be recapitulated in culture which may lead to insights into disease mechanisms and potential treatments.

Significance Statement

This study demonstrates that retinal pigmented epithelial (RPE) cells generated from patients with Sorsby Fundus Dystrophy (SFD) produce highly dysregulated extracellular matrices. SFD RPE form large basal deposits in culture that are similar in composition to what is observed in donated SFD post-mortem globes from family members. Further, SFD RPE demonstrate high levels of 4-hydroxyproline, a major breakdown product of collagen. SFD RPE are also more vulnerable to oxidative stress. Our studies indicate that key elements of SFD pathology can be recapitulated in culture, and ECM dysregulation may lead to metabolic changes detrimental to RPE health.

Introduction

Sorsby Fundus Dystrophy (SFD) is a rare form of autosomal dominant macular degeneration that shares similar clinical features with age-related macular degeneration (AMD). Both SFD and AMD patients develop macular drusen, geographic atrophy, choroidal neovascularization, and progressive central vision loss.[1,2] Individuals with SFD often experience an earlier onset of symptoms compared to their AMD counterparts, which may result in central vision loss by the fourth decade of life. While the pathogenesis of AMD is multifactorial, SFD results from mutations in a single gene, called tissue inhibitor of metalloproteinase 3 (*TIMP3*).

TIMP3 is secreted by the retinal pigment epithelium (RPE), and it plays a critical role in extracellular matrix (ECM) remodeling. It inhibits several matrix metalloproteinases (MMP-1, -2, -3, and -9), a disintegrin and metalloproteinases (ADAMs), and ADAMs with thrombospondin motifs (ADAMTSs).[3,4] TIMP3 also inhibits angiogenesis and inflammation by influencing VEGF-VEGFR2 interactions. [5] While all TIMP family members are secreted, only TIMP3 is sequestered in Bruch's membrane (BrM), a thin layer interposed between the RPE and underlying choriocapillaris.[6]

Bruch's membrane is a semi-permeable barrier that provides structural support for the RPE and allows for nutrient flow from the choriocapillaris. A histological hallmark of SFD is the presence of a grossly thickened and disorganized BrM in post-mortem globes.[7] The thickened BrM was hypothesized to function as a diffusion barrier preventing nutrients from reaching the RPE and retina from the choriocapillaris. SFD patients given high dose vitamin A supplements to counteract this were noted to have some restoration of night vision, albeit at an unsustainably high dose.[8]

While mutant TIMP3 expression is suspected to play a role in the progressive thickening of BrM in SFD and subsequent RPE degeneration, no animal model has robustly reproduced these salient characteristics.[9] However, SFD is an attractive candidate disease for study using patient-derived induced pluripotent stem cell (iPSC) RPE due to its early-onset and clinically severe phenotype attributable to a single gene. The availability of familial SFD post-mortem globes allows for further validation of the SFD iPSC-derived RPE phenotype in culture. The objective of this study is to characterize an iPSC-derived *in vitro* model of SFD that robustly recapitulates ECM dysfunction in order to lend insight into disease pathogenesis and serve as a potentially useful phenotype for the development of therapeutics. Finally, because ECM dysfunction can impact cellular metabolism and susceptibility to oxidative damage [10], metabolic changes in patient-derived SFD RPE and the effects on RPE cell survival are also examined.

Materials and Methods

See Supplement for Expanded Materials and Methods.

Histology of post-mortem globes

Sorsby fundus dystrophy (SFD) globes were generously donated to the Lions Eye Bank of Oregon. Normal adult human globes were obtained from the University of Washington Tissue Bank for Ophthalmology Research (HSD# 41470). Standard protocols for hematoxylin and eosin (H&E), periodic acid-Schiff (PAS), Alizarin red and Movat's pentachrome staining were performed on tissue sections. Images were taken at 40X on a Nikon Eclipse E1000 wide field microscope (Meridian Instrument Company).

Clinical imaging and generation of patient-derived iPSCs

Informed consent was obtained from all participants prior to inclusion in the study, and experiments were conducted according to the principles expressed in the Declaration of Helsinki. Study participants underwent 30° digital fundus color imaging (Zeiss Visucam, Zeiss, Oberkochen, Germany) and optical coherence tomography imaging (Spectralis HRA-OCT; Heidelberg Engineering, Heidelberg, Germany).

Peripheral blood mononuclear cells (PBMC) were obtained from SFD and normal control participants in a University of Washington IRB-approved protocol (HSD#: 43143). iPSC generation from PBMCs was performed as previously described. [11]

CRISPR-Cas9 gene editing of the S204C TIMP3 mutation in SFD patient-derived iPSCs

One million iPSCs derived from individual V-7 harboring the 610A>T (p.Ser204Cys) mutation in the TIMP3 locus were electroporated with Cas9 (0.15uM, Sigma) and gRNA (0.75uM,

Synthego) as RNP complex along with ssDNA donor (4uM, IDT) using Amaxa nucleofector (Human Stem Cell kit 2) in presence of ROCK inhibitor and HDR enhancer (30uM,IDT). Individual colonies were hand-picked and plated into 96 well plates. DNA was extracted using Quick Extract DNA extraction solution (Epicentre#QE09050) and nested PCR was performed. The PCR product was purified using EXO-SAP enzyme (ThermoFisher) and sent for Sanger sequencing analysis (through Genewiz).

RPE differentiation and culture

RPE cell lines were differentiated from iPSCs according to the rapid differentiation protocol and as described previously. [11,12]

Transmission electron microscopy

iPSC-derived RPE cells were cultured for eight weeks on filter inserts and fixed in 4% glutaraldehyde in 0.1M cacodylate buffer. Excised filter membranes were processed according to core facility protocol (see Supplemental Expanded Materials and Methods). For paraffin-embedded SFD globes, approximately 1mm x1mm-sized pieces were deparaffinized with xylene followed by ethanol washes, then PBS. These were then fixed for TEM as described above. Montage TEM images were generated with an average of 27 images per montage, ranging between 91,517.926nm and 126,419.400nm in length. Analyzed images included six control and six SFD montages. Extracellular matrix area and sub RPE deposit dimensions were measured using Fiji software, and ECM area measurements were adjusted for montage length to determine average ECM thickness with standard error. ECM measurements from SFD sections did not include deposits.

Immunocytochemistry and immunohistochemistry

Transverse sections of paraffin-embedded adult SFD and age-matched control globes were placed on glass slides and deparaffinized. Antigen retrieval was performed and tissues were washed with PBS and blocked with 10% horse serum for 1 hour at room temperature. Primary antibody staining was carried out overnight at 4°C. Secondary antibody staining was performed using the corresponding fluorescent-tagged antibodies. Fluoromount-G was used to preserve tissue before coverslips were added to slides and stored in the dark at 4°C. Images were taken at 63x using a Leica DM6000 CS confocal microscope (Leica Microsystems). Transwell filter membranes were fixed in 4% PFA, entered a sucrose gradient, excised from the plastic holder, embedded in O.C.T. compound, and placed in -80°C until sectioning.

Alizarin staining

For alizarin red staining, RPE cells were cultured on 8-well chambered Permanox slides (Nunc Lab-Tek #177445, ThermoFisher Scientific) for 6-8 weeks. Cells were washed two times with 1xDPBS and fixed in 20-30 min 4% PFA prior to Alizarin Red staining. Low power images were taken with an iPhone 5S camera, and higher resolution images at 10-20x on a Nikon Eclipse E1000 wide-field microscope (Meridian Instrument Company). Digital images, with scale set with a cm-scale ruler, were used for quantification of Alizarin positive area per well by Image J/Fiji software. For wells where no deposits were visible, verification was performed with the Nikon Eclipse E1000 wide-field microscope. Multiple wells were quantified using three control, four CRISPR/Cas9 edited, and three SFD RPE lines.

Zymography and reverse zymography

Zymography and reverse zymography were performed as previously described.[13] Cell culture media, cell lysate, and ECM samples were collected from RPE cultured for 8 weeks. In brief, samples were prepared in non-reducing Laemmli sample buffer and separated on a 7.5% SDS-polyacrylamide gel containing 1mg/ml gelatin (zymogram) or using 12% SDS-polyacrylamide gels with 1mg/ml gelatin and RPE cell-conditioned media as a source of MMPs (reverse zymography). After electrophoresis, gels were incubated in a solution of 25mg/ml Triton X-100 to renature proteins. The gels were then washed with water and incubated 16 hrs in 50mM Tris-HCL (pH7.5) containing 5mM $CaCl_2$ and 0.2mg/ml sodium azide at 37°C. Gels were then stained with 5mg/ml Coomassie Blue R-250 in acetic acid/methanol/water (1:3:6) for 2 hrs and destained with acetic acid/methanol/water (1:3:6).

Targeted metabolomics analysis with liquid chromatography and mass spectrometry analysis

After removal of culture media, RPE cells were rinsed once with cold 154mM NaCl solution quickly. 80% methanol pre-chilled in -20^{o}C was added to extract metabolites. The samples were dried and analyzed by liquid chromatography and mass spectrometry (LC MS/MS) as reported previously. [14,15]

Stable isotope-labeled metabolite analysis

RPE cells were replaced with DMEM (without glucose and glutamine, ThermoFisher:# A1443001) supplemented with 1% FBS, 5.5 mM glucose and 200 μM ^{13}C glutamine (Sigma, #605166) or 200 μM ^{13}C proline (Sigma, #604801) for 24 hours. The medium and cells were

collected for gas chromatography–mass spectrometry (GC-MS) as described in detail previously.[11,14,16]

Statistical Analysis

Data are expressed as mean ± SD or SEM as indicated and graphed in GraphPad Prism (Version 7.00 for Mac OS), GraphPad Software, La Jolla California USA, www.graphpad.com or Excel (Microsoft version 16.16.23). Significance of differences between means was determined by unpaired two-tailed t-tests or ANOVA. A *p*-value <0.05 was considered significant (*), <0.01(**), and <0.001 (***). Volcano plot made and analyzed with XLSTAT (2018.1.49540) in Microsoft Excel using unpaired t-test to determine significance.

Results

Family members with the S204C TIMP3 mutation demonstrate clinical and pathological findings of Sorsby Fundus Dystrophy

Members of a large Sorsby Fundus Dystrophy (SFD) family underwent sequencing of exon 5 in the *TIMP3* gene and were assembled in an extensive pedigree, part of which was first reported over twenty years ago (Fig. 1A).[17] Induced pluripotent stem cells (iPSCs) were generated from two individuals, V-2 and V-7, who each carry one copy of the S204C (c.610A>T) mutation. Both patients demonstrated clinical manifestations typical of SFD, although the onset of vision changes, severity of vision loss, and fundus findings varied (Fig. 1B). Individual V-2, a 66-year old woman, experienced loss of central vision in both eyes in her fourth decade as a result of complications from choroidal neovascularization (CNVM). Her best corrected visual acuity (BCVA) was 1/200 in the right eye and 2/200 in the left eye. Color fundus imaging revealed widespread RPE and choroidal atrophy with central macular pigmentary clumping and disciform scarring (Fig. 1B, top image). OCT imaging revealed extensive subretinal scarring with severe overlying macular atrophy (Fig. 1B, bottom image, arrow). Individual V-7, a 63-year old woman, presented with a BCVA of 20/20 in both eyes and was largely asymptomatic upon initial presentation. Four years later, she developed CNVM in the right eye, which was successfully treated without recurrence for over three years with a single injection of intravitreal bevacizumab. She was able to maintain 20/20 vision in that eye. Fundus images of patient V-7 show significant RPE mottling in the macula and large yellow deposits, which were noted most prominently along the vascular arcades and in the mid-periphery. OCT imaging revealed the presence of both conventional drusen (Fig. 1B, white arrow) and subretinal drusenoid deposits (SDD), with the typical peaked morphology (Fig. 1B,

black arrowhead). The presence of reticular pseudodrusen in SFD eyes has been reported previously.[18]

Histology was performed on donated globes from two affected family members, IV-5 and V-13. They were ages 85 and 77 years, respectively, at the time of globe donation, had prior clinical confirmation of SFD, and were genetically confirmed to carry the S204C mutation. Light microscopy revealed significant retinal atrophy and total loss of the outer nuclear layer in some areas. There was also significant disruption of the RPE monolayer with either missing RPE or multiple layers of RPE, and the RPE cells themselves exhibited irregular morphology (Fig. 1C). Most notably, a thick layer of sub-RPE deposits, ranging from ~10-50 μm, was present in all sections extending from the macula to an area just posterior to the ora serrata (Fig. 1C, white double arrowheads). Haematoxylin and eosin (H&E) and periodic acid-Schiff (PAS) staining demonstrated that the deposits were located internal to the elastin layer of Bruch's membrane. Movat's pentachrome staining revealed the presence of mucopolysaccharides and collagen in the sub RPE deposits (Fig. 1C, bottom).

Transmission electron microscopy (TEM) of the sub-RPE deposits in SFD globes showed large regions of electron dense deposits, wide-spaced banded material, and electron-lucent spaces of varying diameter (Fig. 2A). Wide-spaced material with ~80-110 nm periodicity seen in the sub-RPE deposits of SFD globes is presumed to be collagen type VI. [19,20] In some areas, there was an absence of BrM between the sub-RPE deposits and choroidal endothelial cells (CEC) (Fig. 2A), while in others, there was an inner collagenous layer, discontinuous elastic layer, and outer collagenous layer (Fig. 2B). While the overlying RPE were abnormal in overall morphology, the cells maintained apical microvilli and extensive basal infoldings, even

adjacent to the extensive sub-RPE deposits. Phagocytosis of outer segments could be appreciated (Fig. 2B, white arrows), implying some degree of residual RPE function.

Sorsby Fundus Dystrophy iPSC-derived RPE have high levels of intracellular and ECM TIMP3 protein while MMP-2 and -9 activity is unchanged

Three distinct iPSC clones were generated from each of two SFD individuals, V-2 and V-7, and differentiated into RPE. Four RPE cell lines generated from three normal iPSC control subjects were included in these studies. At four weeks in culture, SFD patient and control iPSC-derived RPE cell lines demonstrated characteristic features of mature RPE, including hexagonal morphology, tight junction formation, and the presence of melanin pigment granules as demonstrated by light microscopy and immunostaining with ZO-1 (Fig. 3A). RPE cell lines seeded on filter membranes established tight junctions, and transepithelial resistance (TER) measurements of $\geq 200\Omega \bullet cm^2$ were noted at 4 weeks in culture and were maintained through 12 weeks in culture (Fig. 3B).

We next examined mRNA transcript levels of common RPE-related genes and did not detect a significant difference between expression levels of bestrophin, RPE65, CRALBP, vitronectin, COL6A1, or TIMP3 in SFD-derived RPE compared to controls (Fig. 3C). APOE mRNA expression trended higher in SFD RPE, although it did not reach statistical significance. There was no change in TIMP3 mRNA expression in SFD-derived RPE, which is consistent with *in situ* hybridization results in SFD eyes with the same S204C TIMP3 mutation.[21,22] Despite consistent levels of TIMP3 mRNA expression, TIMP3 protein was observed to be greatly increased in the BrM of SFD patient globes.[19,23] Similarly, SFD iPSC RPE showed ~4-fold higher intracellular TIMP3 protein expression and TIMP3 deposition in ECM compared to

controls (Fig. 3D). Thus, similar to SFD patient globes, SFD iPSC-RPE cultured *in vitro* have unchanged TIMP3 mRNA levels despite highly increased intracellular and ECM TIMP3 protein expression.

We performed zymography to assess the activity of two matrix metalloproteinases (MMPs) commonly found in Bruch's membrane, MMP-2 and MMP-9. Hydrolysis of the gelatin substrate by proteinases is reflected as white bands on a dark background. There was no significant difference in MMP-2 or MMP-9 activity in SFD RPE compared to controls (Fig. 3E). We then examined the inhibitory activity of mutant TIMP3 from SFD cell lysates using reverse zymography (Fig. 3F). In reverse zymography, TIMP3 inhibition of MMP activity is represented by dark bands against a lighter background of digested gelatin.[13] We observed a small decrease in MMP inhibition from SFD RPE (Fig. 3F, top), although when adjusted for levels of TIMP3 protein, SFD TIMP3 displayed a ~5-fold decrease in MMP inhibition compared to controls (Fig 3F, bottom). These results show that while there is significantly greater intracellular and ECM TIMP3 in SFD RPE, mutant TIMP3 is 5-fold less effective at inhibiting MMP-2 and MMP-9.

S204C TIMP3 iPSC-derived RPE form thinner extracellular matrices and elaborate large deposits similar in composition to basal laminar drusen

We next examined the ultrastructure of SFD RPE cultured on polyethylene terephthalate (PET) transwell inserts by TEM. Both control and SFD RPE exhibit features typical of native RPE, including apical microvilli, basal infoldings, pigment granules, and tight junctions (Fig. 4A-C). RPE nuclei were located nearer to the basal surface and oval in shape with the long axis parallel to the basal membrane. PET inserts have been shown to allow the formation of an

extracellular matrix (ECM) on the filter membrane surface.[24] Control iPSC RPE cell lines consistently deposited a uniform layer of fine filaments at the filter interface, which on average measured ~800 nm in thickness (Fig. 4A, top image, arrow). Similar to native RPE basement membrane, the fine filaments do not enter the RPE basal infoldings (Fig. 4B, arrow).[25] In contrast, the layer of filamentous ECM elaborated by SFD RPE was irregular, significantly thinner, and intercalated into the basal infoldings (Figs. 4A, 4C, arrows). Quantification of ECM thickness measurements reveal a 4-fold decrease in SFD RPE ECM thickness compared to that of controls (Fig. 4D).

SFD-derived RPE elaborated large accumulations of extracellular deposits by four weeks in culture (Fig. 4A, asterisks). No deposits were detected in control RPE at the same time point (Fig. 4E). SFD RPE overlying the large deposits maintained apical microvilli, basal infoldings and tight junctions (Fig. 4F). The deposits contained short segment, long spaced transverse bands of 30nm in width and ~110 nm axially repeated periodicity (Fig. 4F"). These complexes were similar in size and architecture to the wide-spaced banded structures seen in sub-RPE deposits of SFD globes (Fig. 4G). Multiple electron lucent vesicles of varying diameter, consistent with lipid, were noted in the culture deposits (Fig. 4F'", white arrowheads), which were similar to those found in SFD globe sub-RPE deposits (Fig. 2A, white arrowheads). While there were rare scattered areas of amorphous, electron dense debris, SFD iRPE deposits did not contain the large electron dense accumulations found in SFD globes (Fig. 4G, d).

SFD iPSC-RPE deposits are similar in composition to sub-RPE deposits in SFD globes

SFD iPSC RPE cultured on chambered slides also formed large sub-RPE deposits, and confocal microscopy with 3D reconstruction imaging revealed the topography of these deposits,

which measured up to ~90μm in elevation (Suppl. Fig.1). The deposits, distinct from sub-RPE fluid pockets that are occasionally observed in mature RPE cell cultures, were difficult to analyze on slides due to poor antibody penetration. We instead performed immunocytochemistry of sub-RPE components on cross sections of RPE cultured on transwell filter membranes. RPE cells express TIMP3 and secrete it into BrM, where it is tightly bound to the extracellular matrix. Increased levels of TIMP3 in BrM have been described in aged eyes and even higher levels have been noted in SFD patients globes.[19,23] Immunostaining of control globes demonstrated TIMP3 in RPE and less prominently in BrM, whereas in SFD globes, there was significant TIMP3 staining in the sub-RPE deposits (Fig. 5A-B). Control and SFD iPSC RPE demonstrated intracellular TIMP3 expression, although TIMP3 was especially notable in the sub-RPE deposits of SFD iPSC RPE (Fig. 5C-D). Immunostaining of basal laminar drusen components including apolipoprotein E (ApoE), vitronectin, clusterin, and collagen type VI was also performed (Fig. 5 and Suppl. Fig. 2). Vitronectin, clusterin, and ApoE were strongly expressed in the thickened sub-RPE deposits of SFD globes and also in the sub-RPE deposits of SFD iPSC RPE (Fig. 5). Immunostaining of collagen type VI, which is associated with basal laminar drusen, was detected both in the RPE and BrM of control and iPSC-RPE and in the sub RPE deposits in SFD globes and SFD iPSC RPE (Suppl. Fig. 2 A-D). TIMP2, an intracellular RPE protein, was not detected in the BrM of control or SFD globes (Suppl. Fig. 2 E-F). As expected, it was also not detected in sub-RPE deposits in SFD iPSC RPE (Suppl. Fig. 2H). Overall the pattern and degree of staining in SFD globes and SFD iPSC RPE deposits are similar among the proteins tested (Suppl. Table 1).

Calcium deposits are found in SFD Globes and SFD iPSC-RPE, while CRISPR-edited iPSC RPE do not form deposits.

Calcium aggregates are found in refractile drusen and in the elastic layer of aged BrM.[25–27] Hydroxyapatite spherules were identified in sub-RPE deposits in older eyes, and porcine RPE form deposits containing hydroxyapatite after aging in culture. [28,29] Alizarin red, an anthroquinone derivative, identifies free calcium and calcium phosphates, in tissues sections and cultured cells. While there was no obvious Alizarin red staining in normal control globes, there was diffuse staining of the thickened BrM and underlying consolidated and enlarged choriocapillaris of SFD eyes (Fig. 6A-B). SFD iPSC RPE cultured on chambered slides for 6 weeks formed significantly more calcium deposits compared to controls (Fig. 6C-D, F). In order to validate the effects of mutant TIMP3 on calcium deposition, CRISPR gene editing was performed on SFD iPSCs to correct the S204C TIMP3 mutation and were differentiated into RPE (Suppl. Fig. 3). Corrected TIMP3 SFD patient-derived iPSC RPE reverted to the control phenotype with significantly fewer deposits (Fig. 6E-F).

S204C TIMP3 iPSC-derived RPE have increased intracellular 4-hypdroxyproline and are more susceptible to oxidative stress

Because cellular metabolism can be affected by disturbances in ECM homeostasis, we examined whether the metabolism of SFD iPSC RPE is altered compared to control RPE. Forty-six key metabolites involved in energy metabolism including glycolysis, mitochondrial Krebs cycle, amino acids, ATP and NADH (Suppl. Table 2) were examined using targeted metabolomics with LC MS/MS. 4-hydroxyproline is the most significantly altered of the metabolites with a ~2.7-fold increase and p-value $\leq 1.0 \times 10^{-8}$ (Fig. 7A). 4-hydroxyproline is a

major component of collagen and required for collagen stability.[30] Its increase could result from either greater synthesis from proline hydroxylation or increased degradation from collagen. To determine if the increase in 4-hydroxyproline was due to increased synthesis, we used a labeled proline tracer. We incubated the RPE cells with labeled ^{13}C proline, but we did not detect a significant difference in the consumption of ^{13}C proline in the cell culture media, implying that the increased 4-hydroxyproline might not be caused by *de novo* synthesis by degradation (Fig 7B).

Glutathione in its reduced state (GSH) is a metabolite that is critical in preventing damage from oxidative stress, and we found that it is significantly decreased by ~3-fold in SFD iPSC RPE compared to controls (Fig. 7A), indicating that SFD RPE may have higher levels of oxidative stress. We previously reported that RPE has an exceptionally high capacity for reductive carboxylation and that reductive carboxylation can play a significant role in RPE resistance to oxidative stress.[11] We traced reductive carboxylation by quantifying ^{13}C labeled metabolites from SFD iPSC RPE and control iPSC RPE incubated with ^{13}C glutamine for 24 hours. The reductive flux in the iPSC RPE cells is as high as mature human primary RPE cells; however, there is no difference in reductive carboxylation between SFD and control iPSC RPE (Fig 7C). SFD RPE cells produce lower levels of ^{13}C-labeled malate and pyruvate but not α-ketoglutarate (Fig 7C). The production of pyruvate through malate is an important source of NADPH which is required for GSH regeneration, indicating that SFD RPE may be more oxidatively stressed at baseline. We did not detect significant changes in the levels of lactate, pyruvate, pentose phosphate pathway intermediates or glucose consumption (Fig. 7A). To determine whether SFD iPSC RPE cells are more sensitive to oxidative damage, SFD and control iPSC RPE were treated with 1mM H_2O_2, a strong oxidative stressor. After 48 hours, there

were more than twice as many dead cells in the SFD iPSC RPE than in control RPE as detected by ethidium homodimer staining (Fig. 7D). Consistently, LDH activity was also highest in the culture media from SFD iPSC RPE cells treated with H_2O_2 (Fig. 7D). Together, these data indicate that SFD iPSC RPE are more oxidatively stressed at baseline and more vulnerable to oxidative damage.

Discussion

Sorsby fundus dystrophy (SFD) retinas are notable for a thick layer of extracellular deposits between the basal lamina of the RPE and the inner collagenous layer of Bruch's membrane (BrM).[7,19,31] Similar to prior publications [32–34], we found that SFD globe deposits contain fibrous long-spaced collagen, lipid, and calcium. Based on their location and composition, these sub-RPE deposits are consistent with basal laminar drusen (BlamD). [35] BlamD are also found in aging retinas, albeit to a much lesser extent than in SFD, and there is a strong relationship between macular BlamD and the formation of exudative age-related macular degeneration (AMD). [36] The accumulation of BlamD causes the RPE to slowly separate from the underlying BrM, likely affecting nutrient transport and RPE function.[8,37]

While no animal model has reproduced the BlamD accumulations seen in SFD patients, our findings show that *in vitro* SFD patient-derived RPE can form large BlamD (up to ~6-90 μm in height) at 60 days, and by as early as 30 days, in culture. The BlamD formed by SFD iPSC RPE are similar in architecture to what is seen in SFD globes, including structures consistent with collagen type VI and lipids. BlamD in AMD globes contain ApoE, vitronectin, clusterin, and fibronectin.[34,38,39] We found these components highly expressed in the BlamD of SFD eyes, and in the sub-RPE deposits of SFD iPSC RPE. RPE cells overlying the distorted BrM in SFD globes appear to retain the ability to phagocytose outer segments, and likewise, SFD iPSC RPE cells overlying large BLamD maintain apical microvilli and tight junctions, implying some remaining function and potential for rescue.

An earlier study described findings of calcium deposition in an SFD globe affected by the same S204C TIMP3 mutation. [19] We found that calcium deposits accumulate in both the BlamD and in the enlarged choriocapillaris in SFD globes. Free calcium and calcium phosphate

deposition by SFD iPSC RPE on chambered slides was especially prominent compared to controls. Although specific mechanisms linking the S204C TIMP3 mutation to extracellular calcium deposition is unclear, the complex array of sub-RPE calcium deposits observed in AMD patients have been proposed to result in part from the release of mitochondrial calcium in failing RPE cells. [28,29,40] We found that TIMP3 gene correction was sufficient to result in reversal of this phenotype *in vitro*. Additional studies on the relationship between ECM homeostasis, RPE stress, and calcium deposition are needed.

ECM and BlamD formed by SFD iPSC RPE described here differ from previously published reports. Prior studies found smaller deposits in older iPSC-RPE cultures[41], and another recent study reported no difference between deposits formed by control and SFD iPSC RPE.[33] In addition, basal deposits have been detected in normal RPE after extended periods of time in culture.[28,39] Possible sources of the disparities among these studies include choice of initial basal substrates (e.g. laminin, Matrigel), time in culture, and non-TIMP3-related genetic modifiers. These factors likely play an important role in RPE disease modeling studies.

In normal aged, AMD, and SFD eyes, increased TIMP3 in BrM is seen without a corresponding increase in TIMP3 mRNA.[21–23,42] A recent study hypothesized that TIMP3 accumulation in SFD RPE may be due to retained protein in the RPE or ECM[33], and our results demonstrate that TIMP3 accumulation occurs in both. It is unclear from prior studies performed in Cos7, ARPE-19, cardiac endothelial cells whether mutant TIMP3 retains the ability to inhibit MMPs.[43,44] We report here that intracellular S204C TIMP3 is ~five-fold less effective at MMP inhibition. Increased ECM degradation is also evidenced by a ~3-fold increase ($p<1.0 \times 10^{-8}$) in 4-hydroxyproline, a collagen degradation product. Reduced mutant TIMP3 activity may lead to a compensatory overproduction of TIMP3, resulting in accumulation in the

ECM and BlamD.

The formation of excessive amounts of basement membrane components may be a general epithelial cell response to stress in order to remain adherent. [45] We found that the SFD RPE are more oxidatively stressed at baseline and have a 3-fold decrease in reduced glutathione, a critical metabolite in preventing damage from oxidative stress. A recent *in vivo* study of a different SFD-associated TIMP3 mutation (S179C) murine model supports this finding, as low doses of sodium iodate, an oxidizing agent, resulted in RPE and photoreceptor degeneration.[46] Disruption of ECM homeostasis likely results in an environment of increased oxidative stress that contributes to disease onset and progression.

Conclusion:

This study demonstrates that mutant TIMP3 results in ECM dysregulation and increased oxidative stress in RPE cells. These results enhance our understanding of the SFD pathology and shed new light on disease mechanisms.

Acknowledgements

The authors wish to thank Ed Parker for assistance with TEM imaging, C. Dirk Keene for histology interpretation, Rayne Lim for help with the graphical abstract, Kelie Gonzalez for cell culturing. We also would like to thank Julie Mathieu, Chris Cavanaugh, and Jennifer Hesson in the Tom & Sue Ellison Stem Cell Core for assistance with CRISPR gene editing.

Disclosure of Potential Conflicts of Interest

The authors have nothing to disclose.

Data Availability Statement

Data is reported in figures, materials and methods, or supplemental material. Additional information is available upon request from authors.

Funding

NIH Grants EY026030 (J.D., J.B.H., and J.R.C.), EY06641 (J.B.H.), EY017863 (J.B.H.), EY019714 (J.R.C.), and EY001730 (National Eye Institute Vision Research Core); BrightFocus Foundation (J.D., J.R.C.); Illinois No. 3 Foundation (J.R.C.); Retinal Research Foundation (J.D.); the Bill & Melinda Gates Foundation (J.R.C.); RPB Sybil B. Harrington Physician-Scientist Award for Macular Degeneration (J.R.C.), Illinois No. 3 Foundation Grant (J.R.C.), and an unrestricted grant from Research to Prevent Blindness (J.R.C.), EY016490 (BA-A), EY027083 (BA-A), EY020861 (BA-A), and P30EY025585 (Cole Eye Institute).

References

1 Anand-Apte B, Chao JR, Singh R, et al. Sorsby fundus dystrophy: Insights from the past and looking to the future. Journal of Neuroscience Research 2019;97:88–97.

2 Weber BHF, Vogt G, Wolz W, et al. Sorsby's fundus dystrophy is genetically linked to chromosome 22q13-qter. Nature Genetics 1994;7:158–161.

3 Arpino V, Brock M, Gill SE. The role of TIMPs in regulation of extracellular matrix proteolysis. Matrix Biology 2015;44–46:247–254.

4 Stöhr H, Anand-Apte B. A review and update on the molecular basis of pathogenesis of Sorsby fundus dystrophy. Advances in Experimental Medicine and Biology, vol. 723, 2012:261–267.

5 Qi JH, Anand-Apte B. Tissue inhibitor of metalloproteinase-3 (TIMP3) promotes endothelial apoptosis via a caspase-independent mechanism. Apoptosis 2015;20:523–534.

6 Jackson HW, Defamie V, Waterhouse P, et al. TIMPs: Versatile extracellular regulators in cancer. Nature Reviews Cancer 2017;17:38–53.

7 Kuntz CA, Jacobson SG, Cideciyan A v., et al. Sub-retinal pigment epithelial deposits in a dominant late-onset retinal degeneration. Investigative Ophthalmology and Visual Science 1996;37:1772–1782.

8 Jacobson SG, Cideciyan A v., Regunath G, et al. Night blindness in Sorsby's fundus dystrophy reversed by vitamin A. Nature Genetics 1995;11:27–32.

9 Weber BHF, Lin B, White K, et al. A mouse model for sorsby fundus dystrophy. Investigative Ophthalmology and Visual Science 2002;43:2732–2740.

10 Bonnans C, Chou J, Werb Z. Remodelling the extracellular matrix in development and disease. Nature Reviews Molecular Cell Biology 2014;15:786–801.

11 Du J, Yanagida A, Knight K, et al. Reductive carboxylation is a major metabolic pathway in the retinal pigment epithelium. Proceedings of the National Academy of Sciences of the United States of America 2016;113:14710–14715.

12 Buchholz DE, Pennington BO, Croze RH, et al. Rapid and Efficient Directed Differentiation of Human Pluripotent Stem Cells Into Retinal Pigmented Epithelium. STEM CELLS Translational Medicine 2013;2:384–393.

13 Qi JH, Dai G, Luthert P, et al. S156C mutation in tissue inhibitor of metalloproteinases-3 induces increased angiogenesis. Journal of Biological Chemistry 2009;284:19927–19936.

14 Du J, Linton JD, Hurley JB. Probing Metabolism in the Intact Retina Using Stable Isotope Tracers. Methods in Enzymology, vol. 561, 2015:149–170.

15 Zhu S, Yam M, Wang Y, et al. Impact of euthanasia, dissection and postmortem delay on metabolic profile in mouse retina and RPE/choroid. Experimental Eye Research 2018;174:113–120.

16 Wang Y, Grenell A, Zhong F, et al. Metabolic signature of the aging eye in mice. Neurobiology of Aging 2018;71:223–233.

17 Carrero-Valenzuela RD, Klein ML, Weleber RG, et al. Sorsby fundus dystrophy: A family with the Ser181Cys mutation of the tissue inhibitor of metalloproteinases 3. Archives of Ophthalmology 1996;114:737–738.

18 Gliem M, Müller PL, Mangold E, et al. Reticular Pseudodrusen in Sorsby Fundus Dystrophy. Ophthalmology 2015;122:1555–1562.

19 Chong NHV, Alexander RA, Gin T, et al. TIMP-3, collagen, and elastin immunohistochemistry and histopathology of Sorsby's fundus dystrophy. Investigative Ophthalmology and Visual Science 2000;41:898–902.
20 Knupp C, Chong NHV, Munro PMG, et al. Analysis of the collagen VI assemblies associated with Sorsby's fundus dystrophy. Journal of Structural Biology, vol. 137, 2002:31–40.
21 Bailey TA, Alexander RA, Dubovy SR, et al. Measurement of TIMP-3 expression and Bruch's membrane thickness in human macula. Experimental Eye Research 2001;73:851–858.
22 Chong NHV, Kvanta A, Seregard S, et al. TIMP-3 mRNA is not overexpressed in Sorsby fundus dystrophy. American Journal of Ophthalmology 2003;136:954–955.
23 Fariss RN, Apte SS, Luthert PJ, et al. Accumulation of tissue inhibitor of metalloproteinases-3 in human eyes with Sorsby's fundus dystrophy or retinitis pigmentosa. British Journal of Ophthalmology 1998;82:1329–1334.
24 Sorkio A, Hongisto H, Kaarniranta K, et al. Structure and barrier properties of human embryonic stem cell-derived retinal pigment epithelial cells are affected by extracellular matrix protein coating. Tissue Engineering - Part A 2014;20:622–634.
25 Hogan M, Alvarado J, Weddell J. Histology of the Human Eye. Philadelphia: WB Saunders, 1971.
26 Davis WL, Jones RG, Hagler HK. An electron microscopic histochemical and analytical X-ray microprobe study of calcification in Bruch's membrane from human eyes. Journal of Histochemistry and Cytochemistry 1981;29:601–608.
27 Suzuki M, Curcio CA, Mullins RF, et al. Refractile drusen: Clinical imaging and candidate histology. Retina 2015;35:859–865.
28 Pilgrim MG, Lengyel I, Lanzirotti A, et al. Subretinal pigment epithelial deposition of drusen components including hydroxyapatite in a primary cell culture model. Investigative Ophthalmology and Visual Science 2017;58:708–719.
29 Thompson RB, Reffatto V, Bundy JG, et al. Identification of hydroxyapatite spherules provides new insight into subretinal pigment epithelial deposit formation in the aging eye. Proceedings of the National Academy of Sciences of the United States of America 2015;112:1565–1570.
30 Gordon MK, Hahn RA. Collagens. Cell and Tissue Research 2010;339:247–257.
31 Capon MRC, Polkinghorne PJ, Fitzke FW, et al. Sorsby's pseudoinfiammatory macula dystrophy—sorsby's fundus dystrophies. Eye (Basingstoke) 1988;2:114–122.
32 Curcio CA. Soft drusen in age-related macular degeneration: Biology and targeting via the oil spill strategies. Investigative Ophthalmology and Visual Science 2018;59:AMD160–AMD181.
33 Hongisto H, Dewing JM, Christensen DR, et al. In vitro stem cell modelling demonstrates a proof-of-concept for excess functional mutant TIMP3 as the cause of Sorsby fundus dystrophy. Journal of Pathology 2020;252:138–150.
34 Wang L, Clark ME, Crossman DK, et al. Abundant lipid and protein components of drusen. PLoS ONE 2010;5.
35 Sarks S, Cherepanoff S, Killingsworth M, et al. Relationship of basal laminar deposit and membranous debris to the clinical presentation of early age-related macular degeneration. Investigative Ophthalmology and Visual Science 2007;48:968–977.

36 Khan KN, Borooah S, Lando L, et al. Quantifying the separation between the retinal pigment epithelium and bruch's membrane using optical coherence tomography in patients with inherited macular degeneration. Translational Vision Science and Technology 2020;9:1–11.

37 Zhang Q, Chrenek MA, Bhatia S, et al. Comparison of histologic findings in age-related macular degeneration with RPE flatmount images. Molecular Vision 2019;25:70–78.

38 Curcio C. Pathophysiology of Non-Neovascular Age-Related Macular Degeneration: The Oil Spill in Bruch's Membrane and beyond. Ophthalmologica 2012;228:23–25.

39 Johnson L v., Forest DL, Banna CD, et al. Cell culture model that mimics drusen formation and triggers complement activation associated with age-related macular degeneration. Proceedings of the National Academy of Sciences of the United States of America 2011;108:18277–18282.

40 Tan ACS, Pilgrim MG, Fearn S, et al. Calcified nodules in retinal drusen are associated with disease progression in age-related macular degeneration. Science Translational Medicine 2018;10.

41 Galloway CA, Dalvi S, Hung SSC, et al. Drusen in patient-derived hiPSC-RPE models of macular dystrophies. Proceedings of the National Academy of Sciences of the United States of America 2017;114:E8214–E8223.

42 Kamei M, Hollyfield JG. TIMP-3 in Bruch's membrane: Changes during aging and in age-related macular degeneration. Investigative Ophthalmology and Visual Science 1999;40:2367–2375.

43 Christensen DRG, Brown FE, Cree AJ, et al. Sorsby fundus dystrophy – A review of pathology and disease mechanisms. Experimental Eye Research 2017;165:35–46.

44 Langton KP, McKie N, Smith BM, et al. Sorsby's fundus dystrophy mutations impair turnover of TIMP-3 by retinal pigment epithelial cells. Human Molecular Genetics 2005;14:3579–3586.

45 Khan KN, Mahroo OA, Khan RS, et al. Differentiating drusen: Drusen and drusen-like appearances associated with ageing, age-related macular degeneration, inherited eye disease and other pathological processes. Progress in Retinal and Eye Research 2016;53:70–106.

46 Wolk A, Upadhyay M, Ali M, et al. The retinal pigment epithelium in Sorsby Fundus Dystrophy shows increased sensitivity to oxidative stress-induced degeneration. Redox Biology 2020.

Figure legends

Figure 1. Clinical imaging and histological findings of individuals with S204C *TIMP3* Sorsby Fundus Dystrophy. (A) Abridged pedigree of the SFD family. Filled black symbols indicate individuals with SFD determined by clinical examination. Filled grey symbols are individuals reportedly affected based on family history or likely affected based on inheritance patterns. Open symbols indicate unaffected individuals or those of unknown status. Slashed symbols indicate deceased individuals. Dots indicate genetic confirmation of disease status (black, performed in this study; grey, performed outside of this study). §, individuals from whom iPSCs were generated; *, individuals who donated globes. (B) Retinal imaging of the left eyes of SFD patients. (Left) Color fundus photographs reveal extensive RPE and choroidal atrophy with subretinal scarring, the latter also seen on OCT (white arrow, left bottom). (Right) Macular RPE pigment mottling and yellow deposits in the macula and along the vascular arcades and mid-periphery were observed in color fundus photos. Both conventional drusen (white arrow, right bottom) and conical-shaped subretinal drusenoid deposits (black arrowhead) were noted on OCT imaging. (C) SFD family member globes demonstrate marked deposition of sub-RPE material. There is a thick layer of deposits internal to the elastin layer of Bruch's membrane in SFD eyes (white double arrowheads) seen on hematoxylin and eosin (H&E) and periodic acid-Schiff (PAS) staining. Movat's pentachrome stain demonstrates the presence of mucopolysaccharides (blue-green) and collagen (yellow) in the sub RPE deposits and a thickened and disrupted elastin (black) sublayer of Bruch's membrane in SFD eyes. Scale bar = 25 µm

Figure 2. Transmission electron microscopy of SFD globes have abnormal RPE morphology and disruption of Bruch's membrane. (A) RPE with irregular morphology is shown overlying a thick layer of electron dense deposits (A, white asterisk). RPE basal laminar infoldings (BLI) (A') located adjacent to electron dense deposits (EDD) (A', white asterisk), wide-spaced banded collagen (BC) of 110nm periodicity (A', black arrow), and vesicular structures (V) (A', white arrowhead). Bruch's membrane was absent between the electron dense deposits and choroidal endothelial cells (CEC) in areas (A), while other areas demonstrate a disorganized Bruch's membrane external to the deposits (B, B" inset, left of separation artifact, black asterisk). Abundant collagen fibrils (CF) are noted between the large electron dense deposits (B", black arrow) and the residual discontinuous elastic layer (EL) of Bruch's membrane (B", black arrowhead). Phagocytosis of photoreceptor outer segments by RPE cells overlying large deposits imply some residual function (B', white arrows).

Figure 3. Characterization of SFD iPSC-RPE demonstrates specific changes to TIMP3 protein expression and activity. (A) Brightfield images and immunofluorescent staining show typical RPE pigmentation, hexagonal morphology, and presence of tight junctions in both control and SFD iPSC RPE cells. DAPI, nuclear stain; ZO-1, tight junction marker (B) Control and SFD iPSC RPE demonstrate transepithelial resistance (TER) measurements of at least $\geq 200\Omega \cdot cm^2$ by 4-5 wks in culture. (C) mRNA transcript levels of RPE-related genes between control and SFD RPE. (D) Western blot of RPE cell lysates and ECM show a >4-fold increase in intracellular TIMP3 expression and ECM in SFD RPE compared to controls. Western blot quantification combines glycosylated and unglycosylated TIMP3. (E) Zymography shows no significant difference in either MMP-2 or MMP-9 activity in the media from SFD RPE compared to

controls. (F) Reverse zymography demonstrates TIMP3 inhibition of MMP activity. While there was only a small difference in overall MMP inhibition between SFD and controls (top), there is a ~5-fold decrease in the inhibitory activity of mutant TIMP3 compared to control TIMP3 after adjusting for TIMP3 expression (bottom). Mean+/- SD; *$p<0.05$; **$p<0.005$, ***$p<0.0005$; n=3.

Figure 4. SFD iPSC-derived RPE form irregular extracellular matrices and large basal deposits in culture. (A) SFD RPE cultured for 60 days on polyethylene filter inserts form large basal deposits as seen on TEM montage images (asterisks). (B) Control RPE elaborate a uniform layer of ECM at the filter interface (black arrow) while (C) SFD RPE form irregular and significantly thinner filamentous ECM (white arrow). (D) SFD ECM is approximately 4-fold thinner compared to controls. (E) Quantification of basal deposits revealed significantly increased basal laminar deposits in SFD RPE. (F) One representative sub-RPE deposit measures 15μm in length and 6μm in height. Overlying RPE cells maintain typical ultrastructural features including apical microvilli, basal infoldings and tight junctions (F'). Sub-RPE deposits contain short segmented, long-spaced transverse bands of 30nm in width and ~110 nm axially repeated periodicity, consistent with banded collagen (F"). Electron lucent vesicles of varying diameter were also noted in the deposits (F'", white arrowheads). (G) TEM image of SFD globe demonstrates the presence of banded similar wide-spaced banded structures. Scale bars, as indicated. n, nucleus; r, RPE; d, electron dense deposits; c, choroid. Mean+/- SD; $p<0.05$; n=3 (6 control and SFD RPE cell lines each)

Figure 5. SFD iPSC-RPE deposits in culture are similar in composition to sub-RPE deposits seen in SFD patient globes. Immunostaining of control and SFD globes was compared to control and SFD iPSC-RPE cells cultured on PET filter inserts. (A-D) Intracellular TIMP3 was detected in the RPE (A-B, asterisks) and to a lesser extent in the Bruch's membrane of control globes (A, arrowhead). Sub-RPE deposits seen in SFD globes were strongly immunoreactive for TIMP3 (B, arrow), similar to what is seen in SFD iPSC-RPE deposits (D, arrow). Intracellular TIMP3 was noted in control iPSC-RPE (C, asterisk). ApoE immunostaining was observed in the BrM of control globes (A, arrowhead), sub RPE deposits of SFD globes (B, arrow), and in the sub-RPE deposits of SFD iPSC-RPE (D, arrow). (E-H) Vitronectin and clusterin staining was observed in the RPE and BrM of control globes and were strongly expressed in the thickened sub-RPE deposits in SFD globes (E-F). Similarly, both were highly expressed in the sub-RPE deposits of SFD RPE (H). Scale bars, 10 μm.

Figure 6: *Calcium deposits are found in SFD Globes and SFD iPSC-RPE, while CRISPR-edited iPSC RPE do not form deposits.* (A-B) Alizarin red staining demonstrates calcium accumulation in the sub-RPE deposits and disorganized choriocapillaris. c, choriocapillaris; *artefactual separation (C-D) SFD iPSC RPE cultured on slides form large sub-RPE deposits that stained intensely with Alizarin red compared to their control counterparts. (E) CRISPR-corrected TIMP3 iPSC RPE cells revert to control phenotype. (F) Quantification of calcium deposition by area of Alizarin red staining per well. Bottom, 10x Brightfield images, scale bar 500μm. ****$p<0.0001$; n=9 (3-4 control, SFD, and CRISPR-edited SFD RPE lines each)

Figure 7. SFD iPSC-derived RPE have altered metabolism and are more susceptible to oxidative stress. (A) Metabolite analysis of SFD RPE represented in a volcano plot (vertical red line at 1 and -1 represent 2-fold increase and decrease, respectively; horizontal red line represents *p*-value of 0.05). SFD RPE have ~2.5 fold higher levels of hydroxyproline ($p < 1.0x10^{-8}$), a major product of collagen degradation. SFD RPE cells had 3-fold lower glutathione (GSH) levels. Significant changes in other metabolites include (1) tyrosine, (2) aspartate, (3) alanine, (4) glutamate, (5) fumarate, (6) GTP, (7) FAD, (8) GSSG, (9) choline. (B) SFD RPE, incubated with labeled ^{13}C proline, did not demonstrate a significant increase in ^{13}C proline consumption. (C) Reductive carboxylation was examined by quantifying ^{13}C labeled metabolites from RPE incubated with ^{13}C glutamine. Although there was no change in reductive flux, the flux to malate and pyruvate was significantly attenuated in SFD RPE. (D) Control and SFD RPE cultured for 7-8 weeks were treated with 1mM H_2O_2 for 48 or 72 hours. Cell death was quantified at 48 and 72 hrs by LDH activity and ethidium homodimer staining. *P<0.05 vs Con without treatment and $^{\#}$P<0.05 vs Con with H_2O_2. Data are mean ± SD, $n = 4$. Scale bar = 200 µm.

Supplemental Figure 1. Confocal images with 3D reconstruction of (A) control and (B) SFD iPSC-RPE cultured on chambered slides. (A'-A") Bestrophin (red) was used to label RPE, and scattered vitronectin staining was seen in control RPE cultures (A', arrow). (B) Sub-RPE deposits formed by SFD iPSC RPE measured up to ~90µm in height (white arrowhead). (B'-B") Vitronectin was detected just below the RPE basal surface (white arrows). Areas of steep or irregular morphology in the deposits were unable to be imaged and are indicated with a white asterisk (B-B'). A' and A", B' and B" represent x and y axis images. Horizontal and vertical scale bars, as noted.

Supplemental Figure 2. SFD iPSC-RPE deposits in culture are similar in composition to sub-RPE deposits seen in SFD patient globes. (A-D) Immunostaining of collagen type VI was noted intracellularly in the RPE and in BrM (A, arrowhead) of control globes. Collagen VI was diffusely distributed throughout the thickened BrM in SFD globes (B, arrow). iPSC-RPE deposits stained intensely for Collagen VI (D, arrow). (E-H) TIMP2, a non-secreted intracellular RPE protein, was detected in the RPE (asterisks) and not in BrM. In contrast to ApoE (arrows), TIMP2 was not detected in the thickened BrM of SFD globes (F) or in the sub-RPE deposits formed by SFD iPSC RPE (H). Bestrophin and CRALBP are intracellular RPE markers. Scale bars, 10 μm.

Supplemental Figure 3. Correction of 610A>T TIMP3 mutation using CRISPR-Cas9 in patient-derived iPSCs. (A) Schematic of the genome editing strategy used to repair a point mutation found in patients in the TIMP3 locus. The sgRNA is marked in red, and the PAM sequence is presented in blue. The cutting site of the CRISPR-Cas9 enzyme is indicated by a black arrow. The patient-mutated base in the green square was replaced with the wild type base, producing a single precise point mutation thus resulting in the repair of the disease-causing mutation. A silent mutation was introduced in the PAM region to prevent further cutting by Cas9, as indicated. The long sequence below is a single stranded DNA (ssDNA) donor with the desired repair mutations and homologous arms (45□bp on each side). **(**B-C**)** Sanger sequencing results of TIMP3 in V-7 iPSC line harboring the 610A>T (Ser204Cys) mutation (B) and after correction (C).

Supplemental Table 1. Summary of globe and iPSC-RPE immunostaining

Supplemental Table 2. Metabolites detected by LC MS in RPE

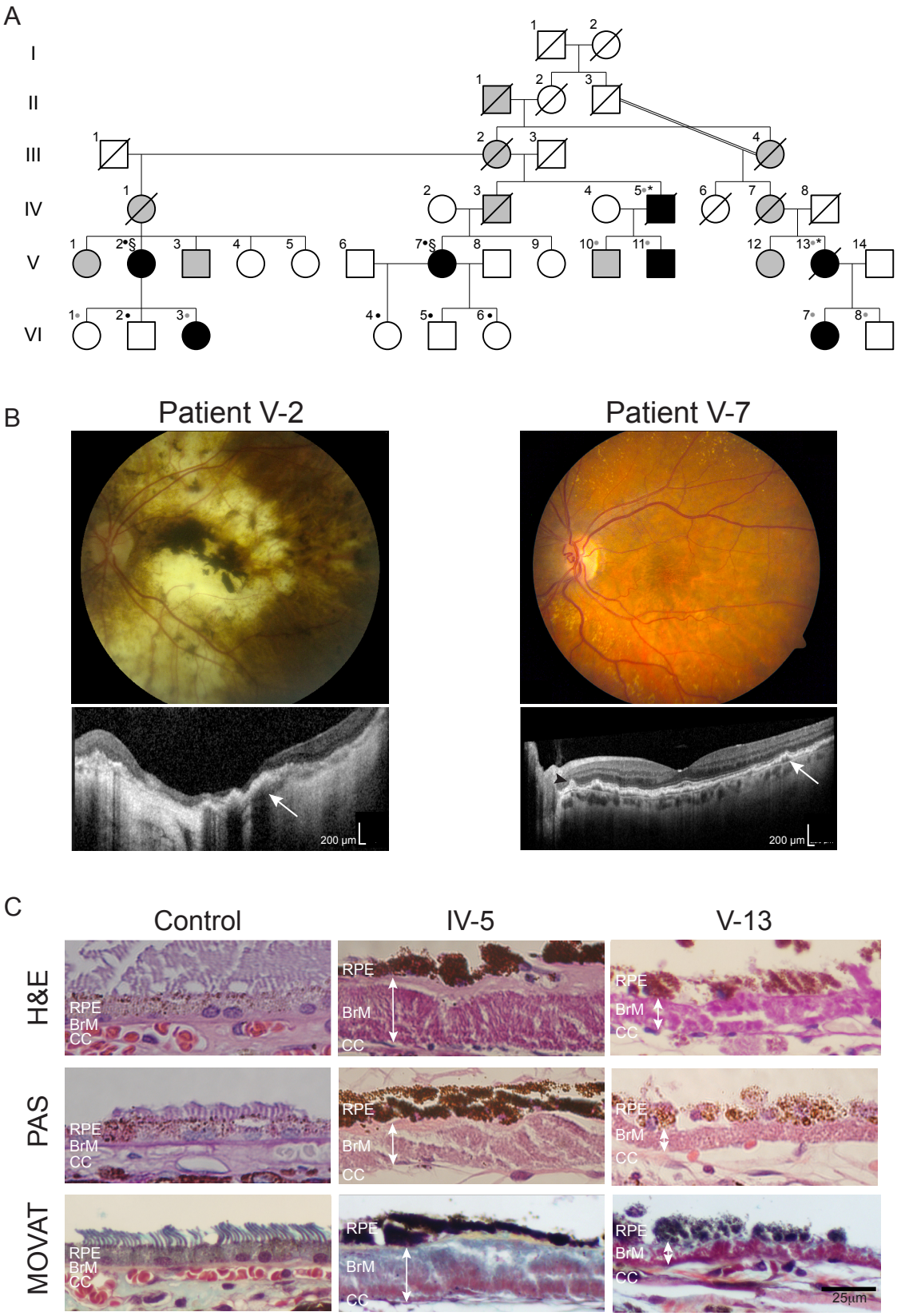

Figure 1

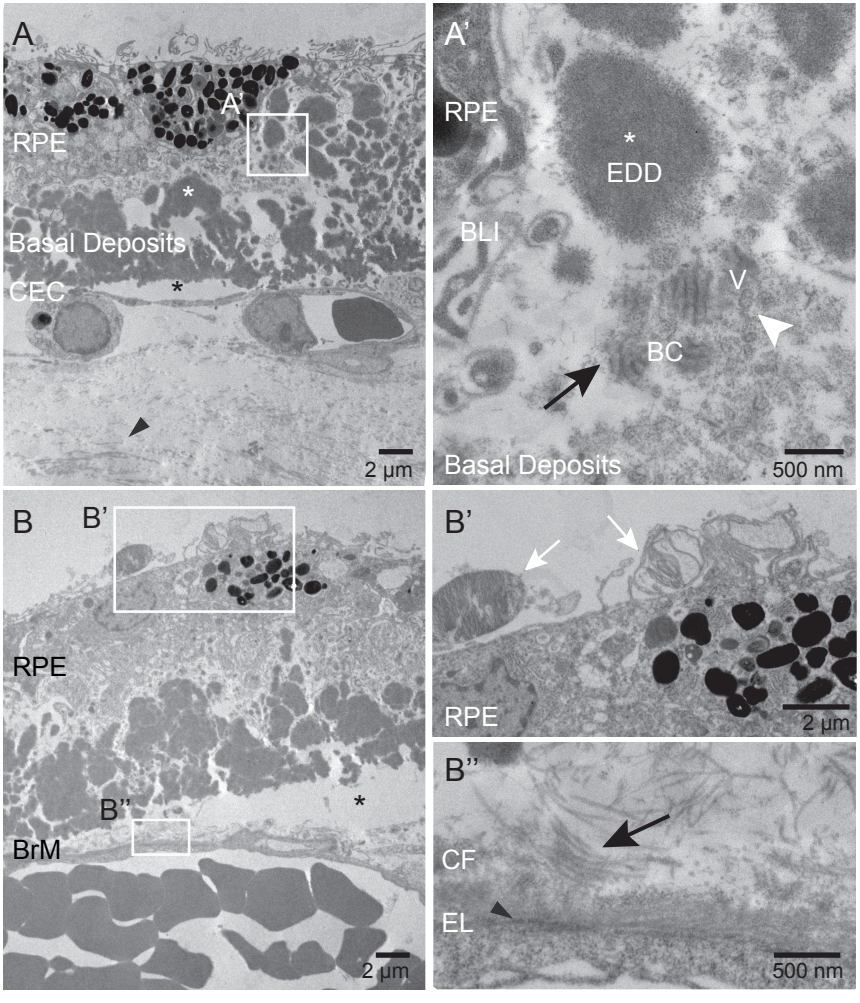
A
A'
RPE
*
Basal Deposits
CEC
*
2 µm
A'
RPE
*
EDD
BLI
V
BC
Basal Deposits
500 nm
B
B'
RPE
B''
*
BrM
2 µm
B'
RPE
2 µm
B''
CF
EL
500 nm

Figure 2

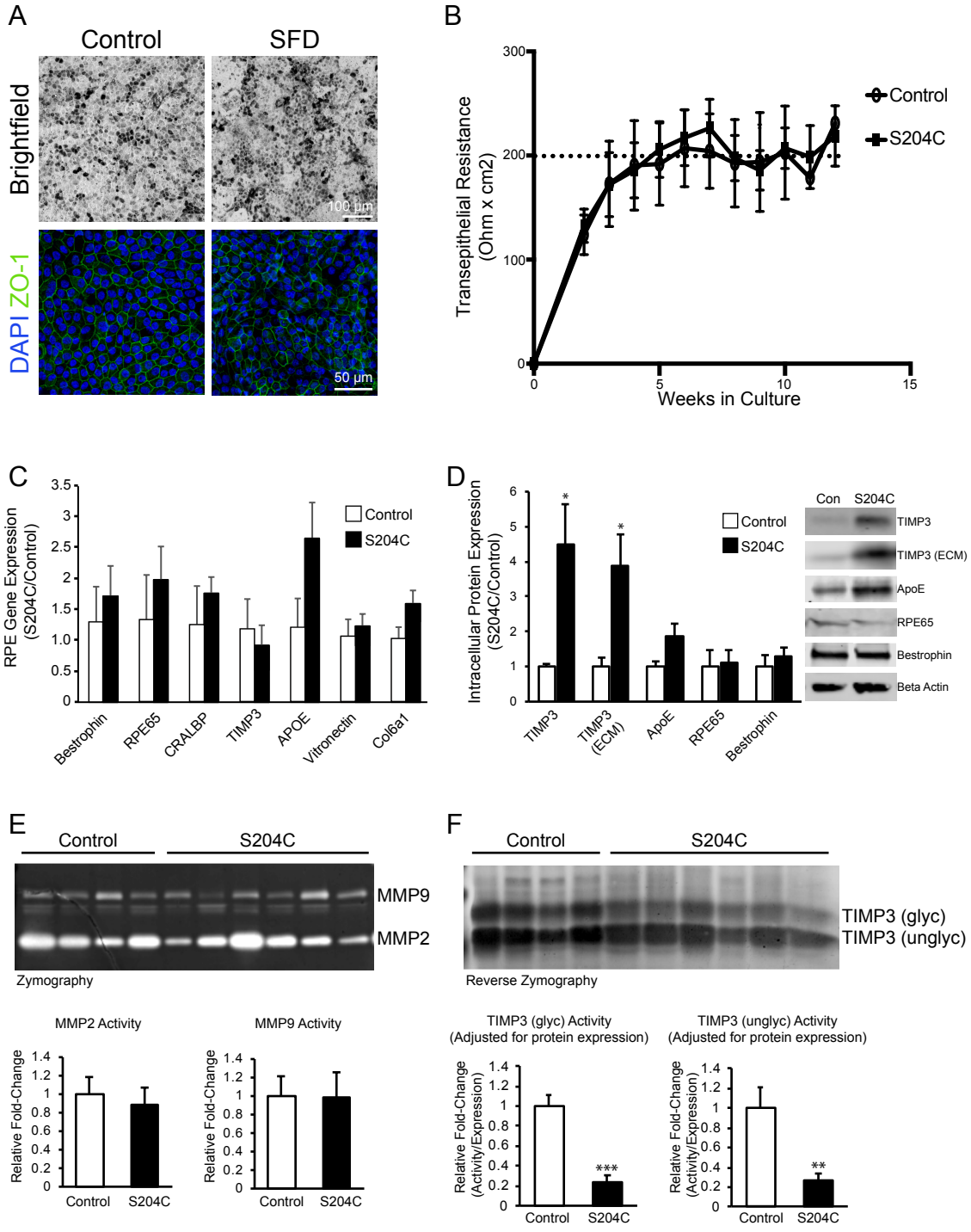

Figure 3

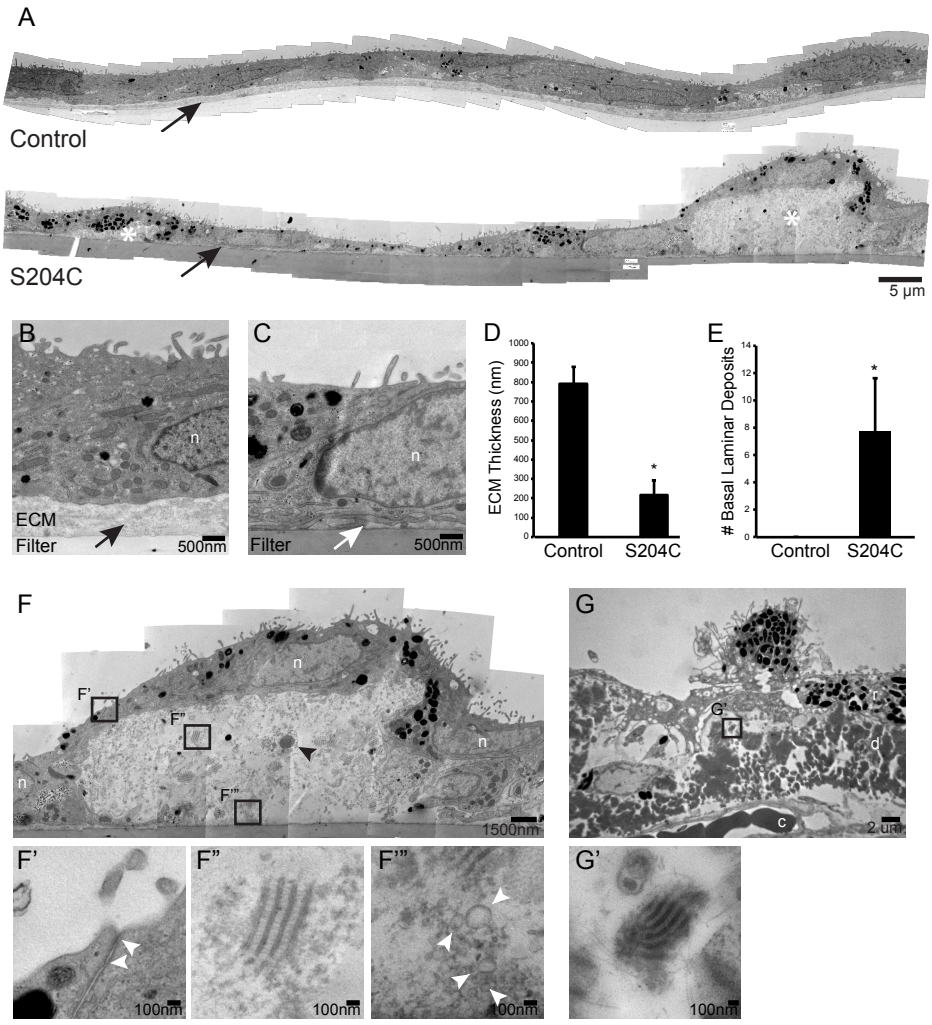

Figure 4

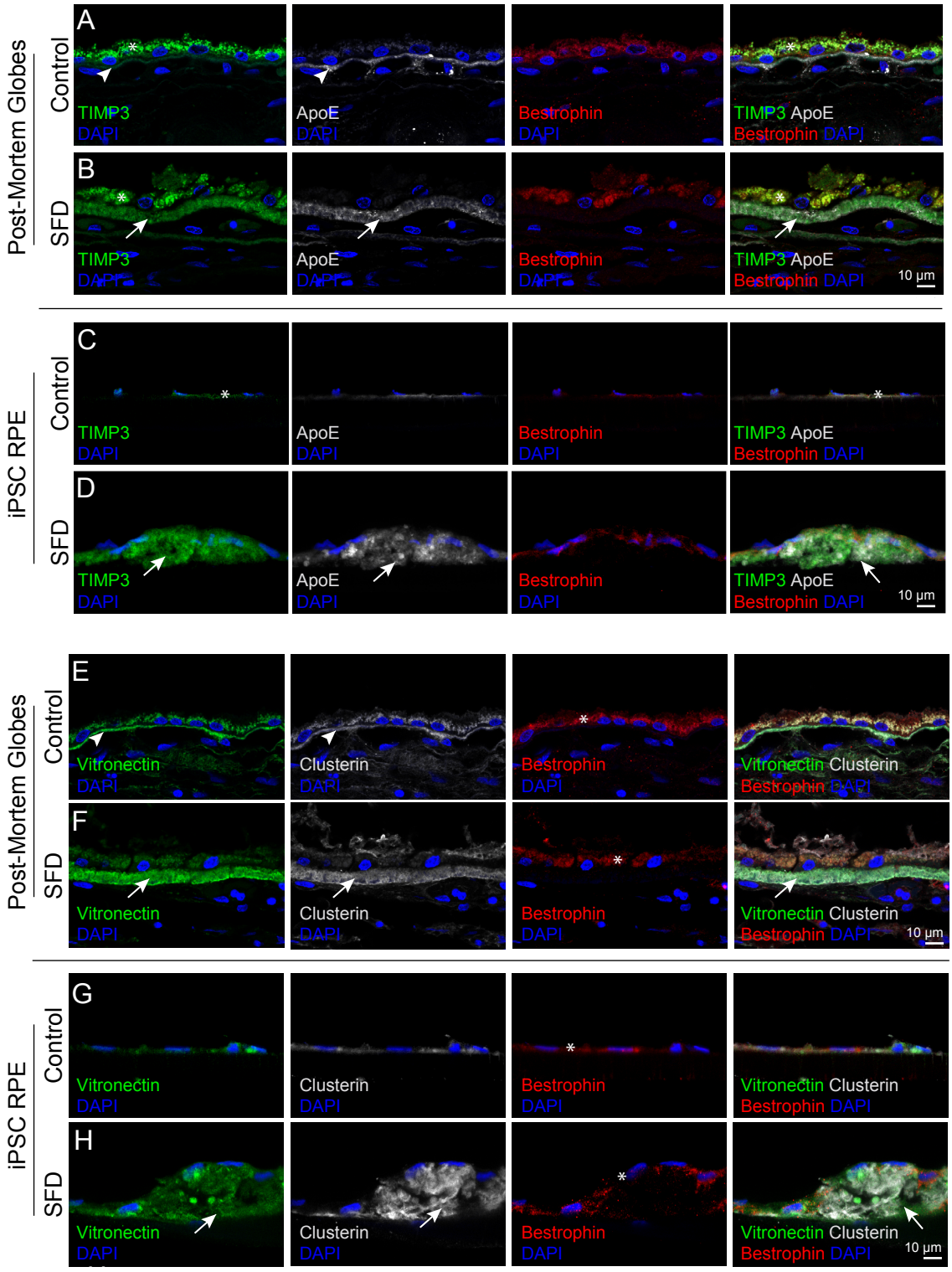

Figure 5

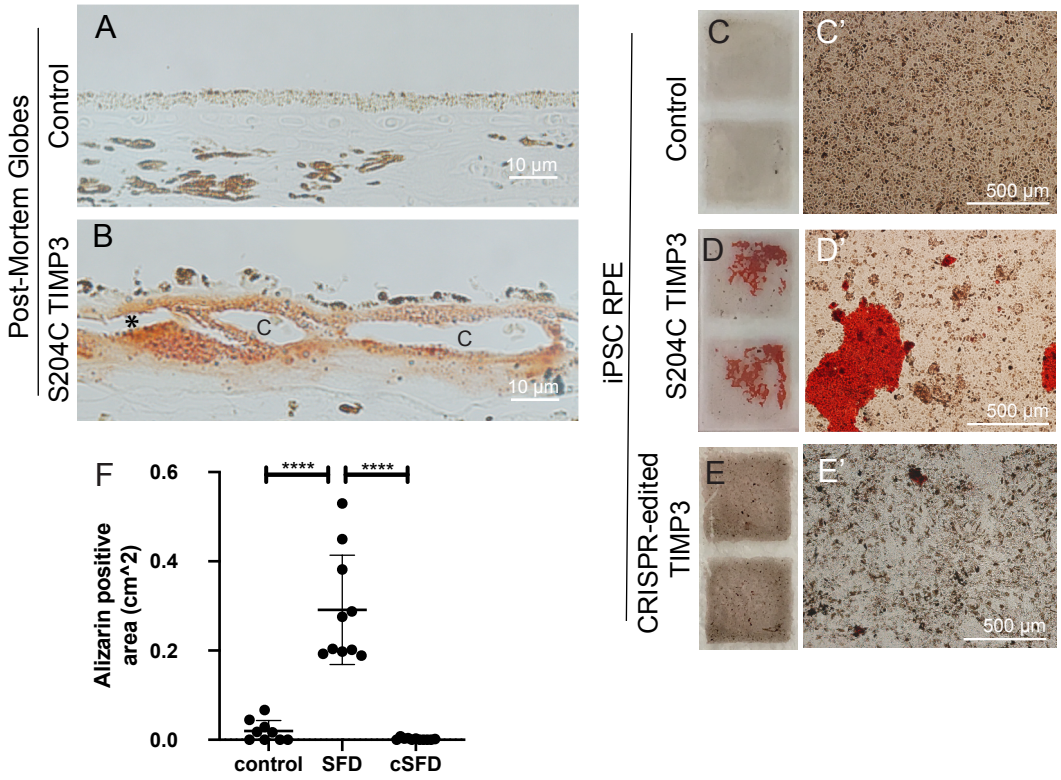

Figure 6

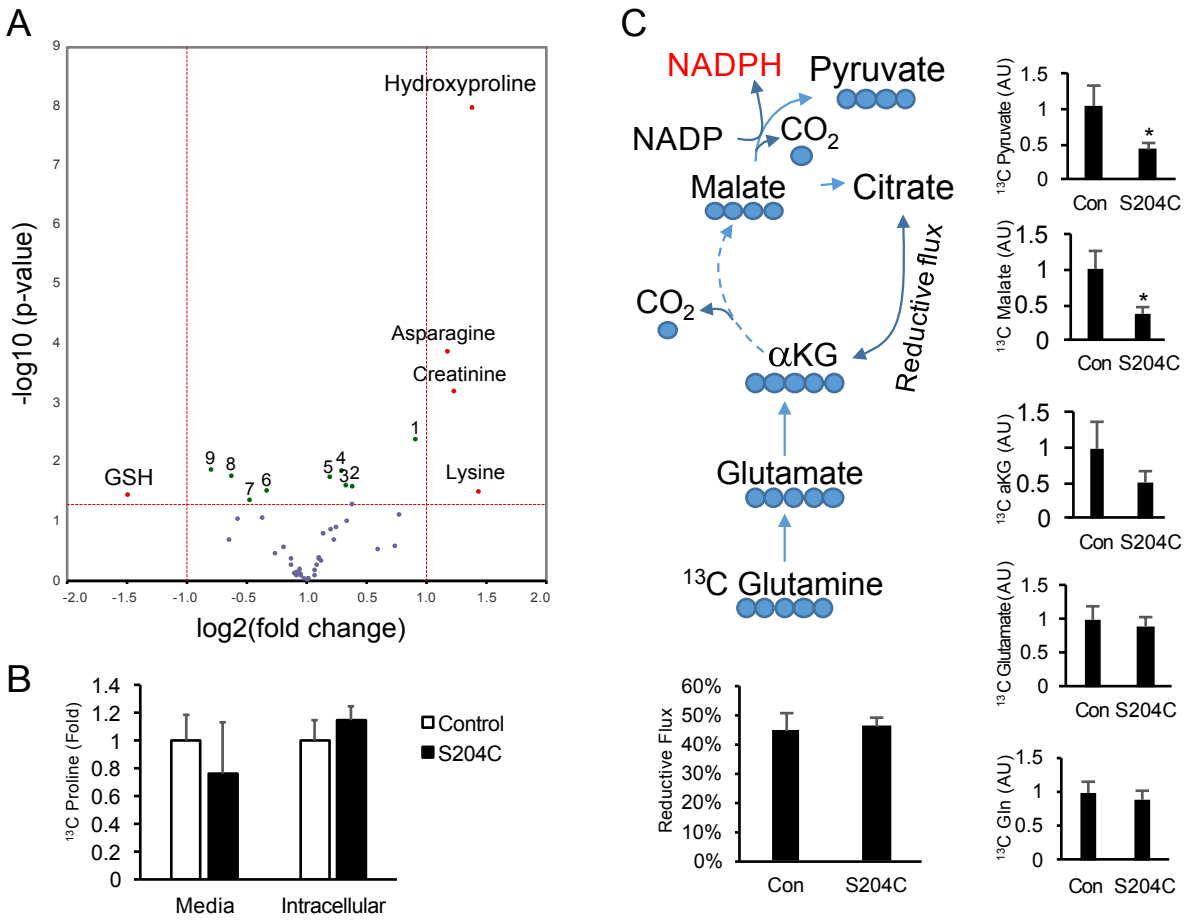

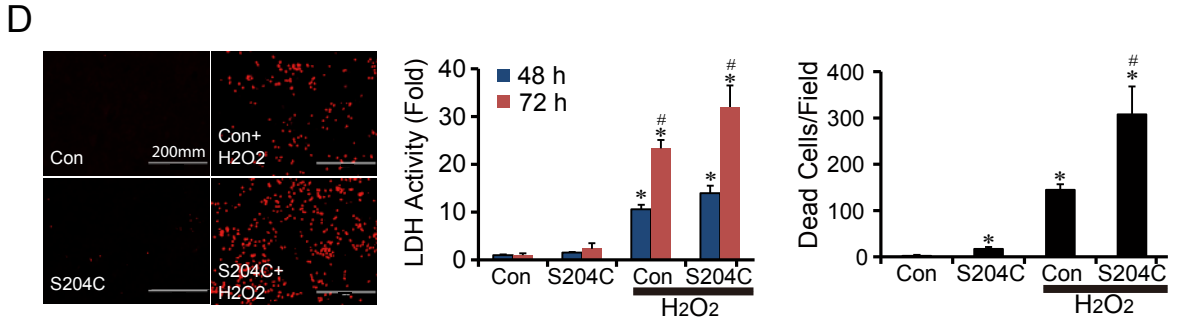

Figure 7